

PAPER • OPEN ACCESS

## *In-situ* bandaged Josephson junctions for superconducting quantum processors

To cite this article: Alexander Bilmes *et al* 2021 *Supercond. Sci. Technol.* **34** 125011

View the [article online](#) for updates and enhancements.

### You may also like

- [A curvature-independent high-resolution pressure sensor provides sub-bandage pressure measurement in accordance with Laplace's law](#)  
Luke A Parkinson, Anthony W Papageorgiou and John W Arkwright
- [Poly \(3-hydroxyalkanoates\)-co-\(6-hydroxyhexanoate\) hydrogel promotes angiogenesis and collagen deposition during cutaneous wound healing in rats](#)  
Ahmad Mohammed Gumel, Mohd Rafais Mohd Razaif-Mazinah, Siti Nor Syairah Anis et al.
- [Towards the development of active compression bandages using dielectric elastomer actuators](#)  
S Pourazadi, S Ahmadi and C Menon



**IOP | ebooks™**

Bringing together innovative digital publishing with leading authors from the global scientific community.

Start exploring the collection—download the first chapter of every title for free.

# *In-situ* bandaged Josephson junctions for superconducting quantum processors

Alexander Bilmes<sup>1,\*</sup> , Alexander K Händel<sup>1</sup>, Serhii Volosheniuk<sup>2</sup>, Alexey V Ustinov<sup>1,3,4</sup> and Jürgen Lisenfeld<sup>1</sup>

<sup>1</sup> Physikalisches Institut, Karlsruhe Institute of Technology, 76131 Karlsruhe, Germany

<sup>2</sup> Kavli Institute of Nanoscience, Delft University of Technology, 2628 CJ Delft, Netherlands

<sup>3</sup> National University of Science and Technology MISIS, Moscow 119049, Russia

<sup>4</sup> Russian Quantum Center, Skolkovo, Moscow 143025, Russia

E-mail: [abilmes@google.com](mailto:abilmes@google.com)

Received 19 August 2021

Accepted for publication 26 September 2021

Published 29 October 2021



CrossMark

## Abstract

Shadow evaporation is commonly used to micro-fabricate the key element of superconducting qubits—the Josephson junction. However, in conventional two-angle deposition circuit topology, unwanted stray Josephson junctions are created which contribute to dielectric loss. So far, this could be avoided by shorting the stray junctions with a so-called bandage layer deposited in an additional lithography step, which may further contaminate the chip surface. Here, we present an improved shadow evaporation technique allowing one to fabricate sub-micrometer-sized Josephson junctions together with bandage layers in a single lithography step. We also show that junction aging is significantly reduced when junction electrodes are passivated in an oxygen atmosphere directly after deposition.

Supplementary material for this article is available [online](#)

Keywords: Josephson junction, micro fabrication, superconducting qubit, shadow evaporation technique, transmon, thin film, superconductivity

(Some figures may appear in colour only in the online journal)

In superconducting quantum processors, qubits are realized with non-linear resonators formed by capacitively or inductively shunted Josephson tunnel junctions [1, 2]. It is commonly understood that dielectric loss in insulation layers and tunnel junction barriers contributes strongly to energy relaxation [3]. Even without deposited dielectrics, surface oxides

and contamination at electrode interfaces are major limiting factors for qubit coherence [4–7].

Qubits require submicrometer-sized Josephson junctions to enhance the circuit's non-linearity, and to minimize the amount of lossy dielectric in the junction's tunnel barriers [3, 9]. Usually, such junctions are made using electron-beam patterning of photoresist to form a Dolan-bridge [10, 11], an intersection of narrow trenches [12–14], or asymmetric undercuts [15]. The shadow cast by these structures when metal is evaporated from two different angles then defines the junction area. After the junction's bottom electrode has been deposited, it is oxidized to form the tunnel barrier, and capped by the top electrode in the second evaporation step. Typically, submicrometer-sized junctions are fabricated on top

\* Author to whom any correspondence should be addressed.



Original Content from this work may be used under the terms of the [Creative Commons Attribution 4.0 licence](#). Any further distribution of this work must maintain attribution to the author(s) and the title of the work, journal citation and DOI.

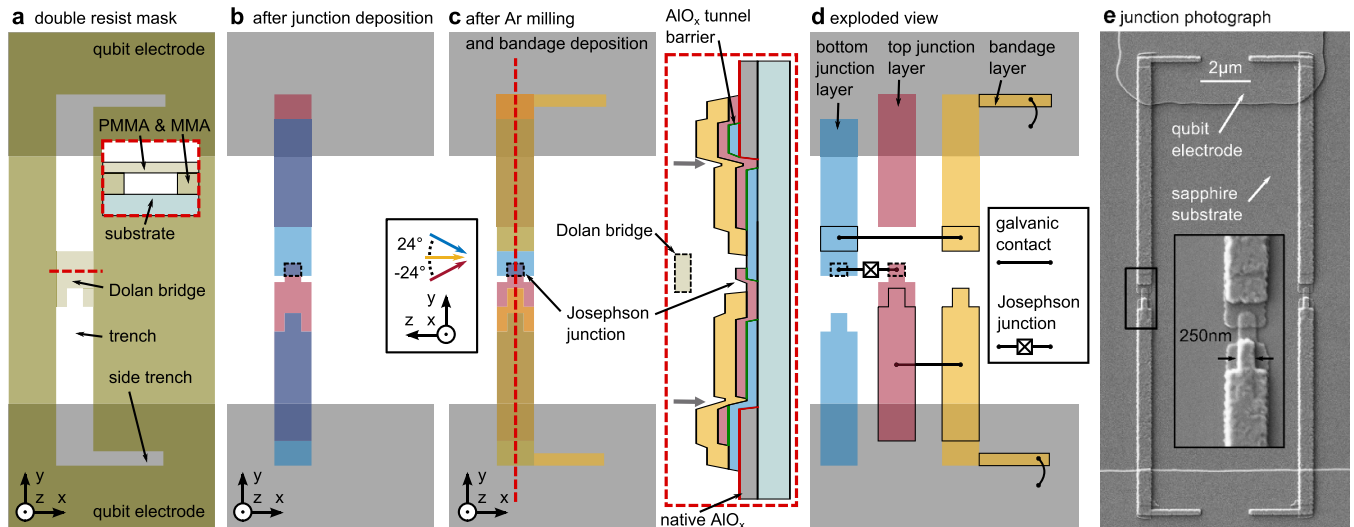


**Figure 1.** (a) Sketch of the double resist mask (developed in cold 2-Propanol [8]), and the Dolan bridge (see inset) for the fabrication of *in-situ* bandaged Josephson junctions. For clarity, the resist mask is not shown in the following sketches. (b) The Josephson junction (dashed rectangle) is created after deposition of a first (red) and second (blue) Al layers at tilted angles (see inset) and an intermediate oxidation which forms the tunnel barrier. Note that no material is deposited in the bottom of the side-trenches visible in (a). (c) Without breaking the vacuum, the aluminum oxide is cleaned from the qubit electrodes (gray) and the junction films by argon ion milling, and a bandage film is deposited perpendicularly to the wafer. The inset shows a cross-section of the junction layers (not to scale) along the red dashed line. (d) The exploded view reveals the chain of galvanic contacts which interconnects the qubit electrodes through the Josephson contact. (e) Electron-microscopy image of a DC-SQUID consisting of two *in-situ* bandaged Josephson junctions, connected to the electrodes of a transmon qubit.

of pre-patterned larger circuit structures such as shunt capacitors, which are made with faster UV-optical lithography [16].

Since the electrodes of the qubit's shunt capacitor are also oxidized during tunnel barrier formation, they are connected to the junction's top electrode through unwanted additional, so-called 'stray' junctions. The contribution of stray junctions to the qubit Hamiltonian is made negligible when they are much larger than the qubit junctions [17]. Increasing the area of the stray junction also reduces the ac-voltage drop across them and thus limits dielectric loss due to structural defects in their tunnel barriers [18]. Nevertheless, even large stray junctions may still contribute significantly to decoherence [19].

Improved qubit coherence is obtained when stray junctions are shorted using so-called bandages that are deposited in a successive lithography step [5]. However, this requires additional lithography which consumes time and carries the risk of introducing further contamination.

Here, we describe an improved shadow-evaporation technique to fabricate sub-micrometer-sized Dolan bridge Josephson junctions together with bandage layers in a single lithography step by using three-angle evaporation. After junction formation, an argon milling plasma [20] is applied *in-situ* prior to bandage deposition. Importantly, due to the anisotropy of the remote argon plasma, the sub-micrometer Josephson junction is protected in the shadow of the resist mask from damage due to impacting ions. In addition, we observe that junction aging, i.e. the drift of normal-state resistance or superconducting critical current, is significantly reduced when the junction electrodes and the bandage layers are oxidized in a controlled atmosphere directly after their deposition.

We note that a similar bandaging technique has recently been developed independently by Osman *et al* and demonstrated for Manhattan-style Josephson junctions [21].

Figure 1(a) shows the double resist mask used to form *in-situ* bandaged Josephson junctions (ISBJ). The Dolan bridge highlighted in green defines the junction area, underneath of which the two Al-electrodes evaporated from  $\pm 24^\circ$  angles are overlapping, see figure 1(b). Before the second deposition, the bottom electrode is oxidized in a static pressure of 15 mBar for 180 s to form the tunnel barrier. Note that the narrow side trenches are oriented perpendicular to the evaporation direction of the junction electrodes, so that the underlying qubit electrodes (gray) are not exposed as shown in figure 1(b) where the mask has been omitted for clarity.

Next, ion-milling is applied in the same vacuum chamber to sputter the oxide from the Al films. Finally, the bandage is deposited (yellow in figure 1(c)) perpendicularly to the substrate to create a galvanic contact between junction layers and the qubit electrodes through the side trenches. The contact areas and the Josephson contact are indicated in the legend of the exploded view shown in the right panel of figure 1(c). The Dolan bridge protects the junction from the argon milling and from being shorted by the bandage. An image of a dc-SQUID fabricated on sapphire, which consists of two ISBJs, is shown in figure 1(e). See supplementary materials which contain a detailed recipe for the here-studied ISBJs.

Note that the bandage spans possible discontinuities of the junction electrodes at the film edges of the qubit electrodes, which are marked in the inset of figure 1(c) by gray arrows. This simplifies the electrode geometry since no basewire

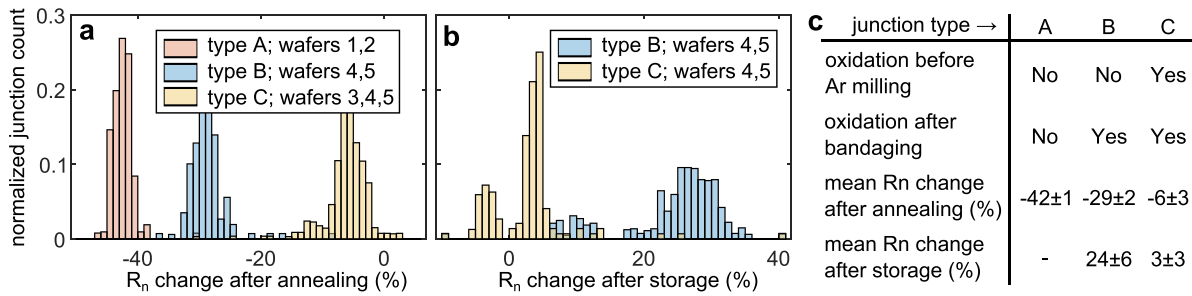


**Figure 2.** (a) Resistance change of *in-situ* bandaged Josephson junctions after thermal annealing (10 min at 200 °C in air). Type B junctions were oxidized *in-situ* after bandaging, while type C junctions were additionally oxidized after junction deposition (10 min at 30 mBar O<sub>2</sub>). Wafers 4 and 5 were cleaved in two after mask development. (b) Resistance change after storage for three weeks at ambient conditions. Type A junctions were not tested. (c) Overview of oxidation steps applied to each junction type, and their resistance change after annealing and storage.

hooks [5] are required which are commonly used to avoid film interruptions.

The critical current density of the junctions is calibrated from measurements of their normal resistance  $R_n$  at room temperature via the empirical relation  $E_t = E_m(R_t/R_n)^{2.5}$  [22] where  $E_m$  is the static oxidation exposure (mBar-s) during tunnel barrier formation,  $R_t$  is the target normal resistance, and  $E_t$  the adjusted oxygen exposure. However, the junction resistance typically shows temporal drift, known as junction aging [23]. To explain aging, it was suggested that the tunnel barrier might incorporate aluminum hydrates [24], where the OH<sup>-</sup>-group may stem from organic resist residuals [25] or from water dissociation at the aluminum oxide interface [6]. It has also been shown that better long-term stability is obtained when junctions are annealed at a few hundred °C temperature in vacuum [23], which was explained by dissociation of aluminum hydrates [24].

We monitored the stability of 500 *in-situ* bandaged junctions (yield > 96%) by measuring their normal resistance  $R_n$  directly after fabrication and after annealing for 10 min at 200 °C in air. Junctions fabricated as described above (type A junctions) showed a resistance drop of  $(42 \pm 2)\%$  after annealing. This might be due to contamination of the junction barrier by resist re-deposition during argon ion milling, and during lift-off in liquid stripper.

The resistance drop after junction annealing was reduced to  $(29 \pm 2)\%$  when the junctions were additionally oxidized *in-situ* after bandaging (type B junctions). Strongest improvement was observed when an additional oxidation step was applied between junction formation and subsequent argon ion milling ('protective oxidation', type C junctions), which reduced the resistance drop to  $(6 \pm 3)\%$ . We speculate that the thicker aluminum oxide may hinder contaminants from diffusing towards the tunnel barrier. Figure 2(a) summarizes the statistics of our observations for the three junction types.

The protective oxidation of junction electrodes also improves the long-term stability during storage. After three weeks at ambient conditions (stored in a laboratory drawer), the resistance of type B junctions increased by  $(24 \pm 6)\%$ , while type C junctions showed an increase of  $(3 \pm 3)\%$  (see figure 2(b)).

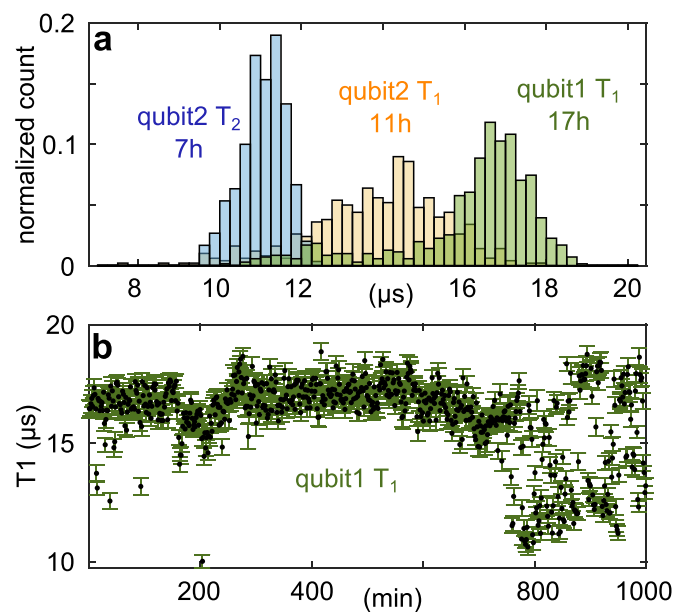


**Figure 3.** (a) Histograms of energy relaxation time  $T_1$  and Ramsey dephasing time  $T_2$  recorded over several hours (the duration is indicated in each histogram label), with two out of three qubits from a same qubit chip. Qubit three was tuned far away from the transmon sweet spot due to trapped vortices. (b)  $T_1$  records vs. time which result in the histogram for qubit No. 1 in the panel above. We recognize that the qubit experienced strong coherence fluctuations in the last three hours of records, most probably due to coupling to some charged tunneling defects [26, 27].

To test the suitability of *in-situ* bandaged Josephson junctions for quantum bits, we used them to fabricate Xmon-type transmon qubits [16, 28]. These had charge and Josephson energies designed to  $E_C \sim 200$  MHz and  $E_J \sim 20$  GHz, respectively. We monitored their energy relaxation times  $T_1$  at qubit resonance frequencies of about 6 GHz during several hours to account for temporal fluctuations due to the interference with material defects [29, 30]. Figure 3(a) shows histograms of  $T_1$  for two tested samples. The obtained average  $T_1$  times were very similar than those we obtained on similarly designed qubits [31] that were fabricated either with

classical shadow junctions [10, 11] or cross-type junctions [13, 32]. Thus, ISBJs did not generate identifiable excess dielectric loss. Figure 3(b) contains the time evolution of  $T_1$  of qubit No. 1, showing strong fluctuations during the last hours of measurement. This is a common issue that is explained by resonance frequency fluctuations of strongly interacting tunneling defects residing on qubit electrodes [26, 27].

We conclude that the presented technique is applicable for fabrication of coherent qubits that are free of stray Josephson junctions, and it works reliably and economizes one lithography step. The reported method also preserves the advantage of conventional bandaging [5] where the interface of junction films to the substrate was not harmed by argon ion milling, and it is slightly simpler than the *in-situ* bandaging technique [21] based on Manhattan-style junctions [12], as it requires a uniaxial wafer tilt for shadow evaporation. Moreover, we observed that the changes of junction resistance induced by thermal annealing and by long-term storage are significantly reduced by adding oxidation steps after junction and bandage layer depositions.

These results offer improvements in the fabrication of stable and contamination-free Josephson junctions as required by quantum-limited parametric amplifiers [33, 34] and superconducting quantum processors. The *in-situ* bandaging technique to avoid parasitic tunnel barriers can also facilitate the deposition of multi-material stacks, e.g. to fabricate superconductor-ferromagnet junctions which have applications in spintronics [35] and superconducting logic circuits [36]. It is also suitable for so-called cross junctions whose bottom layer is deposited separately [9, 13], where the top and bandaging layers can be deposited under distinct wafer orientations.

### Author contributions

The fabrication method and design for ISBJs was developed by A B, and fabricated and tested by A B, S V and A K N. Measurements on qubits were done by J L. The manuscript was written by A B and J L with contributions from all authors.

### Data availability statement

The data that support the findings of this study are available upon reasonable request from the authors.

### Acknowledgments

The authors gratefully acknowledge funding by Google LLC, and support by the KIT-Publication Fund of the Karlsruhe Institute of Technology. A V U acknowledges partial support provided by Rosatom, and the Ministry of Education and Science of the Russian Federation in the framework of the Program to Increase Competitiveness of the NUST MISIS (Contract No. K2-2020-022).

### ORCID iD

Alexander Bilmes  <https://orcid.org/0000-0001-5029-915X>

### References

- [1] Krantz P *et al* 2019 A quantum engineer's guide to superconducting qubits *Appl. Phys. Rev.* **6** 021318
- [2] Kjaergaard M *et al* 2020 Superconducting qubits: current state of play *Ann. Rev. Condens. Matter Phys.* **11** 369–95
- [3] Martinis J M *et al* 2005 Decoherence in Josephson qubits from dielectric loss *Phys. Rev. Lett.* **95** 210503
- [4] Quintana C M *et al* 2014 Characterization and reduction of microfabrication-induced decoherence in superconducting quantum circuits *Appl. Phys. Lett.* **105** 062601
- [5] Dunsworth A *et al* 2017 Characterization and reduction of capacitive loss induced by sub-micron Josephson junction fabrication in superconducting qubits *Appl. Phys. Lett.* **111** 022601
- [6] de Graaf S E *et al* 2017 Direct identification of dilute surface spins on  $\text{Al}_2\text{O}_3$ : origin of flux noise in quantum circuits *Phys. Rev. Lett.* **118** 057703
- [7] Bilmes A *et al* 2020 Resolving the positions of defects in superconducting quantum bits *Sci. Rep.* **10** 1–6
- [8] Rooks M J, Kratschmer E, Viswanathan R, Katine J, Fontana R E and MacDonald S A 2002 Low stress development of poly(methylmethacrylate) for high aspect ratio structures *J. Vac. Sci. Technol. B* **20** 2937–41
- [9] Steffen M *et al* 2006 State tomography of capacitively shunted phase qubits with high fidelity *Phys. Rev. Lett.* **97** 050502
- [10] Niemeyer J and Kose V 1976 Observation of large dc supercurrents at nonzero voltages in Josephson tunnel junctions *Appl. Phys. Lett.* **29** 380–2
- [11] Dolan G J 1977 Offset masks for lift-off photoprocessing *Appl. Phys. Lett.* **31** 337–9
- [12] Potts A, Parker G, Baumberg J and de Groot P 2001 Cmos compatible fabrication methods for submicron Josephson junction qubits *IEE Proc. Sci. Meas. Technol.* **148** 225–8
- [13] Wu X *et al* 2017 Overlap junctions for high coherence superconducting qubits *Appl. Phys. Lett.* **111** 032602
- [14] Kreikebaum J, O'Brien K, Morvan A and Siddiqi I 2020 Improving wafer-scale Josephson junction resistance variation in superconducting quantum coherent circuits *Supercond. Sci. Technol.* **33** 06LT02
- [15] Lecocq F *et al* 2011 Junction fabrication by shadow evaporation without a suspended bridge *Nanotechnology* **22** 315302
- [16] Barends R *et al* 2013 Coherent Josephson qubit suitable for scalable quantum integrated circuits *Phys. Rev. Lett.* **111** 080502
- [17] Stehli A *et al* 2020 Coherent superconducting qubits from a subtractive junction fabrication process *Appl. Phys. Lett.* **117** 124005
- [18] Müller C, Cole J H and Lisenfeld J 2019 Towards understanding two-level-systems in amorphous solids: insights from quantum circuits *Rep. Prog. Phys.* **82** 124501
- [19] Lisenfeld J *et al* 2019 Electric field spectroscopy of material defects in transmon qubits *npj Quantum Inf.* **5** 1–6
- [20] Grünhaupt L *et al* 2017 An argon ion beam milling process for native  $\text{AlOx}$  layers enabling coherent superconducting contacts *Appl. Phys. Lett.* **111** 072601
- [21] Osman A *et al* 2021 Simplified Josephson-junction fabrication process for reproducibly high-performance superconducting qubits *Appl. Phys. Lett.* **118** 064002

- [22] Kleinsasser A W, Miller R E and Mallison W H 1995 Dependence of critical current density on oxygen exposure in Nb-AlO/sub x/-nb tunnel junctions *IEEE Trans. Appl. Supercond.* **5** 26–30
- [23] Koppinen P, Väistö L and Maasilta I 2007 Complete stabilization and improvement of the characteristics of tunnel junctions by thermal annealing *Appl. Phys. Lett.* **90** 053503
- [24] Gates J, Washington M and Gurvitch M 1984 Critical current uniformity and stability of Nb/Al-oxide-Nb Josephson junctions *J. Appl. Phys.* **55** 1419–21
- [25] Pop I-M *et al* 2012 Fabrication of stable and reproducible submicron tunnel junctions *J. Vac. Sci. Technol. B* **30** 010607
- [26] Klimov P V *et al* 2018 Fluctuations of energy-relaxation times in superconducting qubits *Phys. Rev. Lett.* **121** 090502
- [27] Schlör S *et al* 2019 Correlating decoherence in transmon qubits: low frequency noise by single fluctuators *Phys. Rev. Lett.* **123** 190502
- [28] Koch J *et al* 2007 Charge-insensitive qubit design derived from the cooper pair box *Phys. Rev. A* **76** 042319
- [29] Müller C, Cole J H and Lisenfeld J 2019 Towards understanding two-level-systems in amorphous solids: insights from quantum circuits *Rep. Prog. Phys.* **82** 124501
- [30] Burnett J J *et al* 2019 Decoherence benchmarking of superconducting qubits *npj Quantum Inf.* **5** 54
- [31] Bilmes A, Volosheniuk S, Ustinov A V and Lisenfeld J 2021 Probing defect densities at the edges and inside Josephson junctions of superconducting qubits ( arXiv:2108.06555)
- [32] Steffen M *et al* 2006 State tomography of capacitively shunted phase qubits with high fidelity *Phys. Rev. Lett.* **97** 050502
- [33] Sweeny M and Mahler R 1985 A travelling-wave parametric amplifier utilizing Josephson junctions *IEEE Trans. Magn.* **21** 654–5
- [34] Macklin C *et al* 2015 A near-quantum-limited Josephson traveling-wave parametric amplifier *Science* **350** 307–10
- [35] Linder J and Robinson J W 2015 Superconducting spintronics *Nat. Phys.* **11** 307–15
- [36] Feofanov A *et al* 2010 Implementation of superconductor/ferromagnet/superconductor  $\pi$ -shifters in superconducting digital and quantum circuits *Nat. Phys.* **6** 593–7